AN ALGORITHM FOR CONVERTING STATIC EARTH SENSOR MEASUREMENTS INTO EARTH OBSERVATION VECTORS*

Joseph A. Hashmall and Joseph Sedlak
Computer Sciences Corporation
Lanham-Seabrook, Maryland, USA, 20706

ABSTRACT

An algorithm has been developed that converts penetration angles reported by Static Earth Sensors (SESs) into Earth observation vectors. This algorithm allows compensation for variation in the horizon height including that caused by Earth oblateness. It also allows pitch and roll to be computed using any number (>1) of simultaneous sensor penetration angles simplifying processing during periods of Sun and Moon interference.

The algorithm computes body frame unit vectors through each SES "cluster". It also computes GCI vectors from the spacecraft to the position on the Earth's limb where each "cluster" detects the Earth's limb. These body frame vectors are used as sensor observation vectors and the GCI vectors are used as reference vectors in an attitude solution. The attitude, with the unobservable yaw discarded, is iteratively refined to provide the Earth observation vector solution.

INTRODUCTION

Static Earth Sensors[1] (SES) can be used to determine the pitch and roll attitude of Earth pointing spacecraft by detection of the amount of light entering several photocells (eyes). These eyes are directed so that at nominal altitude and attitude the Earth edge intersects with their fields-of-view (FOVs). Any attitude motion will move the eyes with respect to the horizon so that the portion of the FOV intersecting the Earth will change. Therefore the total light (and therefore output current) of the various eyes is a function of the attitude. Because spacecraft yaw moves each eye around the horizon, the SES is quite insensitive to yaw.

A simplified description of the SES serves to illustrate the operation of an SES and provides a definition for some of the terms that will be used later. SESs generally contain clusters of photocells. For complete observability, at least two clusters are required, and the vectors from the body origin to these two clusters can not be coplanar with the Z-axis.

Each cluster contains one or more eyes, usually with triangular FOVs. These eyes measure the position of the Earth limb relative to the spacecraft and, when there are more than one eye, such quantities as the background light level. SESs typically have a passband in the infrared (14-16 microns). In this region of the spectrum the Earth brightness is almost independent of the presence or absence of solar illumination.

The configuration of a SES containing four clusters with four eyes each is shown in Figure 1. The four eyes in each cluster include one that views space and provides a background level, one

* This work was supported by the National Aeronautics and Space Administration (NASA)/Goddard Space Flight Center (GSFC), Greenbelt, MD, Contract GS-35F-4381G, Task Order no. S-71002-G.

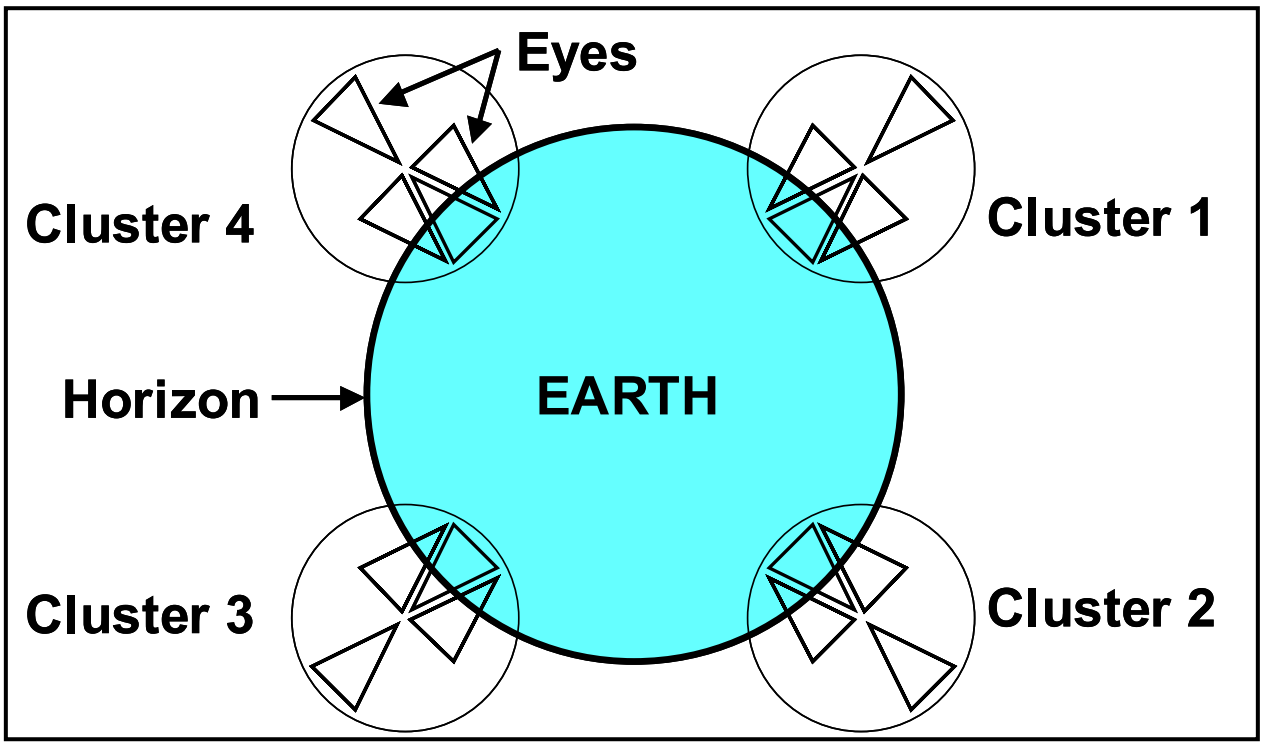

Figure 2. View From Spacecraft to Earth for a Typical SES

that is the primary Earth detection eye (with its broad base towards the Earth) and two that enhance the response of the sensor. The eyes have sides that are typically 5 deg in extent.

The amount of light entering the eyes is expressed as a penetration angle, δ. The penetration angle can be thought of as the angle between the edge of the Earth image in the FOV of the central eye and a reference point. This is illustrated for a simplified SES in Figure 2.

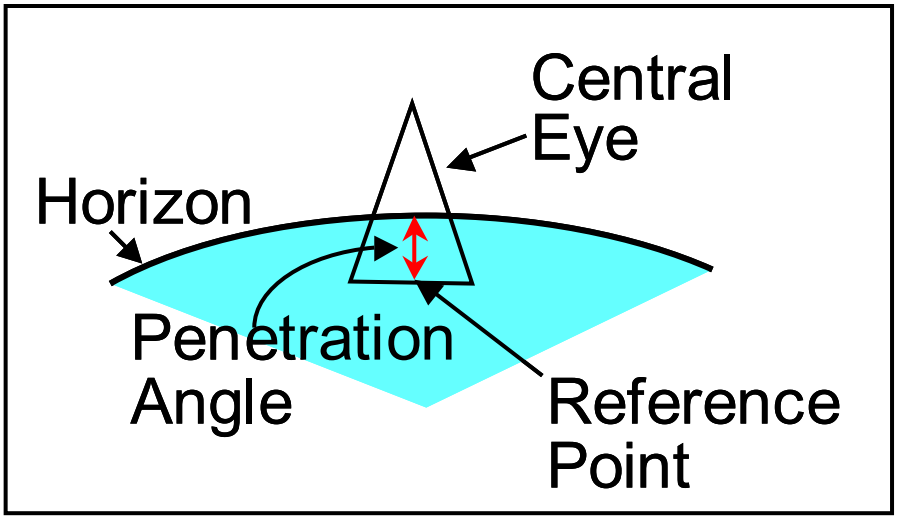

Figure 2. Definition of Penetration Angle For SES

For each cluster, *C*, define a sensor coordinate system: $\hat{X}_C$, $\hat{Y}_C$, and $\hat{Z}_C$ so that:

$$\hat{X}_C = -\frac{\hat{Z} \times \hat{R}_C}{\left|\hat{Z} \times \hat{R}_C\right|} \tag{1}$$

$$\hat{Y}_C = -\frac{\hat{X}_C \times \hat{Z}}{\left|\hat{X}_C \times \hat{Z}\right|} \tag{2}$$

and

$$\hat{Z}_C = \hat{Z} \tag{3}$$

where $\hat{Z}$ is the body Z-axis and $\hat{R}_C$ is a vector from the body origin through the reference point of the cluster. The sensitive direction of the sensor is in the Y_C-Z plane.

The penetration angle for cluster *C* is almost exactly proportional to rotation about $\hat{X}_C$ (the sensitive axis for this cluster) and is relatively insensitive to rotation about $\hat{Y}_C$ (the non-sensitive axis for this cluster). The approximations that the penetration angle is proportional to the first rotation and independent of the second limit the accuracy of the algorithm described in this paper.

For an SES with four clusters, spaced uniformly around the spacecraft Z-axis (the axis that is nominally directed towards Earth), clusters on opposite sides of the spacecraft have antiparallel $\hat{Y}_C$ axes while adjacent clusters have $\hat{X}_2 \equiv \hat{Y}_1$ (with equivalent relationships for the other clusters). Defining rotations about $\hat{Y}_1$ as θ, and those about $\hat{Y}_2$ as ϕ, the attitude can be computed from the penetration angles by:

$$\theta = \frac{(\delta_1 - \delta_3)}{2} \tag{4}$$

and

$$\phi = \frac{(\delta_2 - \delta_4)}{2} \tag{5}$$

where the subscripts indicate the cluster measuring the penetration angle. θ and ϕ can be easily converted to body frame roll and pitch angles using the relationship of the SES coordinate system to the body. Equations (4) and (5) and are used under normal conditions for spacecraft such as the Tropical Rainfall Measurement Mission[2,3] (TRMM).

There are two difficulties with this simple approach to SES attitude determination: compensation for horizon height variation and generality.

Eqs. (4) and (5) are based on the comparison of angles from the Z axis to the detected horizon with angles from the nadir to the horizon. If the Earth appeared spherical in the infrared, nadir-horizon angles would be independent of the location on the Earth where the horizon was detected. The Earth's oblateness causes a latitude and yaw dependent variation in these angles.

Seasonal and position dependent variations in stratospheric temperatures also cause variations of nadir-horizon angles but, unlike oblateness effects, are only approximately predictable.[4]

Oblateness and (if an accurate model is available) stratospheric temperature effects can be compensated by proper adjustment of the penetration angles based on the position and orientation of the spacecraft. This compensation, however, is complex and mission dependent.

Eqs. (4) and (5) are applicable to a specific sensor configuration. The SES must include four clusters and the clusters must be mounted at 90 deg. intervals around the Z-axis. In principal, only two clusters are needed to obtain roll and pitch information and any greater number could be used. In practice, even with four clusters mounted properly, there are times when one or more of the clusters is unavailable (due to Sun or Moon interference). During these times, Eqs (4) and (5) must be replaced by more complex algorithms[5] which are generally also specific to this sensor geometry. The Aqua spacecraft, for example, has an SES with two, non-orthogonal clusters, and consequently requires a different algorithm from these equations.[6]

This paper describes an algorithm that can be used to determine attitudes for a general SES. It is independent of the number and placement of clusters. Using the algorithm, compensation for deviations of the Earth's shape from a sphere is relatively simple. It requires only a model providing the effective Earth radius as a function of time and location on the Earth's surface.

ALGORITHM

The algorithm to determine pitch and roll from SES measurements is iterative. Each iteration consists of the following procedure:

1. *At each time, convert measurement data for each SES cluster into body frame horizon observation vectors, $\hat{O}_C$. These vectors go from the body center through the point in each eye at which the Earth horizon is detected.*

   The body frame vectors, $\hat{R}_C$, are known from the sensor mounting geometry. The body frame observation vectors are calculated by rotation of these vectors around the $\hat{X}_C$-axis by the penetration angle:

   $$\hat{O}_{C,Body} = Rot(\hat{X}_{C,Body}, \delta_C)\hat{X}_C \tag{6}$$

2. *At each time compute Geocentric Inertial (GCI) reference vectors, $\vec{H}_C$, from the spacecraft body to the point on the horizon at which the Earth would be expected to be detected using current estimates of the attitude.*

   2.1. Initially, use nominal values for the pitch and roll. For yaw, use either nominal values or values obtained from another sensor. On subsequent iterations use the most recent attitude estimates for pitch and roll.

   2.2. Using the attitude, convert the vectors $X_{C,Body}$ to GCI:

   $$\hat{X}_{C,GCI} = A^{-1}\hat{X}_{C,Body} \tag{7}$$

   2.3. Compute a horizon crossing vector, $\hat{H}_{C,GCI}$, nearest to $\hat{Y}_C$ from the intersection of two cones. The two cones are:

   one centered on $\hat{X}_{C,GCI}$ with a 90 deg half-angle

one centered on the nadir vector, with-half-angle, ρ, corresponding to the Earth width as viewed from the spacecraft:

$$\rho = \sin^{-1}\left(\frac{r_E + \Delta h}{r_s}\right) \tag{8}$$

where:

- r_E is the Earth equatorial radius,
- Δh is a deviation from the equatorial radius due to the nominal height in the atmosphere at which the sensor detects the Earth, the Earth's oblateness, and any corrections for stratospheric temperature effects
- r_s is the length of the spacecraft nadir vector, $\vec{N}$, to the center of the Earth.

2.4. Scale the horizon crossing unit vector to its appropriate length by:

$$\vec{H}_{C,GCI} = r_s \cos(\rho)\hat{H}_{C,GCI} \tag{9}$$

2.5. Compute the vector from the Earth center to the position on the Earth at which the horizon crossing occurs by:

$$\vec{P}_{C,GCI} = \vec{H}_C - \vec{N} \tag{10}$$

2.6. Obtain Δh_C from $\vec{P}_C$ and some horizon height model. The horizon height may be constant, or variable, based on the time, latitude, and possibly longitude of each horizon crossing position. Normally, it will include oblateness compensation at a minimum. A separate Δh_C is computed for each observation.

2.7. Compute new values of ρ_C and $\vec{H}_C$ (using the values of Δh_C for Δh in Eq. (8)), by repeating steps 2.3 and 2.4. Only a single repetition of these steps is needed because Δh does not vary greatly with position (see below).

3. Solve for attitude using all valid $\hat{H}_C$ and $\hat{O}_C$ vectors. The $\hat{H}_C$ vectors are treated as reference vectors and the $\hat{O}_C$ vectors as observations. The attitude is computed using the QUEST[7] algorithm.
4. Since the yaw rotation is very poorly observable by the SES alone, rotate the computed attitude so that its Z-component is nominal or equal to the input yaw.
5. Repeat steps 2 to 4 until the attitudes no longer change. This generally requires 3 or 4 iterations.
6. Report the X and Y rotations of the final attitude as roll and pitch.

RESULTS

The algorithm was tested using simulated data. Two arrangements of clusters were simulated. The first arrangement has four clusters at 90 deg intervals around the Z-axis. They are located equidistant from the X and Y axes. In cases where only two clusters were used, adjacent clusters were selected. For most of the tests, the two clusters were a pair on the same side of the Y-Z plane, but in one test the two chosen were on the same side of the X-Z plane.

The second arrangement for testing used three clusters. This arrangement placed one cluster in the Y-Z plane and the other two at 120 deg intervals around the Z-axis.

The simulation used an ephemeris from the Aqua mission. Aqua's orbit is nearly circular with a semi-major axis of 7070 km and an inclination of 98.2 deg.

Simulated truth attitudes were created from ten-term Fourier series using random coefficients. Separate coefficients were used for roll, pitch, and yaw attitude components. The range of the coefficients was chosen so that the minimum period of any term was 18 deg and the total amplitudes of the attitudes were about 1 deg.

The pitch, roll, and yaw angles created in this way had maximum values of 1.10, 1.02, and 1.07 deg. and minimum values of -1.24, -1.11, and -1.19 deg, respectively. Their standard deviations were 0.404, 0.352, and 0.402 deg.

The simulated attitudes were sampled at 4 second intervals over a 24 hour period providing 21601 points for each test case. For each point, the penetration angles were simulated using the Aqua ephemeris and an oblate Earth model with a constant horizon height of 30 km above the oblate spheroid. An example of the truth attitude for a portion of the data is given in Figure 3.

In addition to the number and geometry of the clusters, three parameters were varied:

- The number of iterations of the entire algorithm was varied to determine convergence. The number of iterations for finding the horizon height at each location (step 2) was kept at 2. Separate tests showed that the maximum change in Δh was 20.82 km for the first iteration of step 2, 0.095 km for the second, and 0.006 km for the third.
- In some cases, a yaw value of zero was used in the simulation while in others the variable yaw (described above) was applied.
- In some cases a zero-mean, random, gaussian noise with standard deviation of 0.02 deg was applied to the penetration angles.

Examples of the results of some of the cases studied are shown in Figures 4-7 and a summary, providing the maximum absolute differences between truth and calculated attitude components, as well as their standard deviations and the time taken for the computation, is given in Table 1.

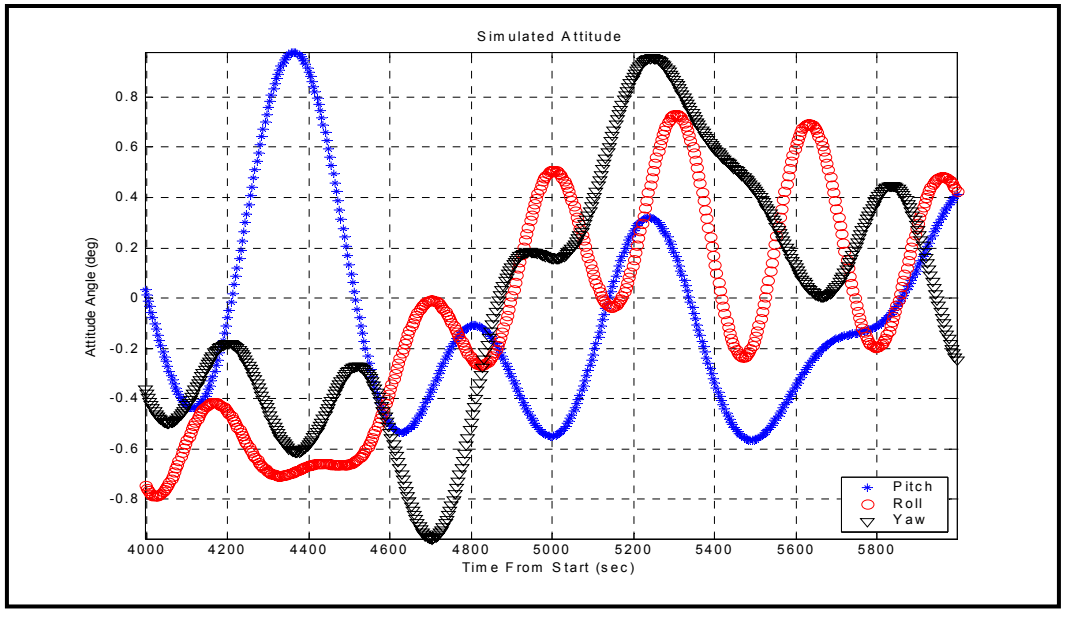

Figure 3. Portion of Simulated Attitude

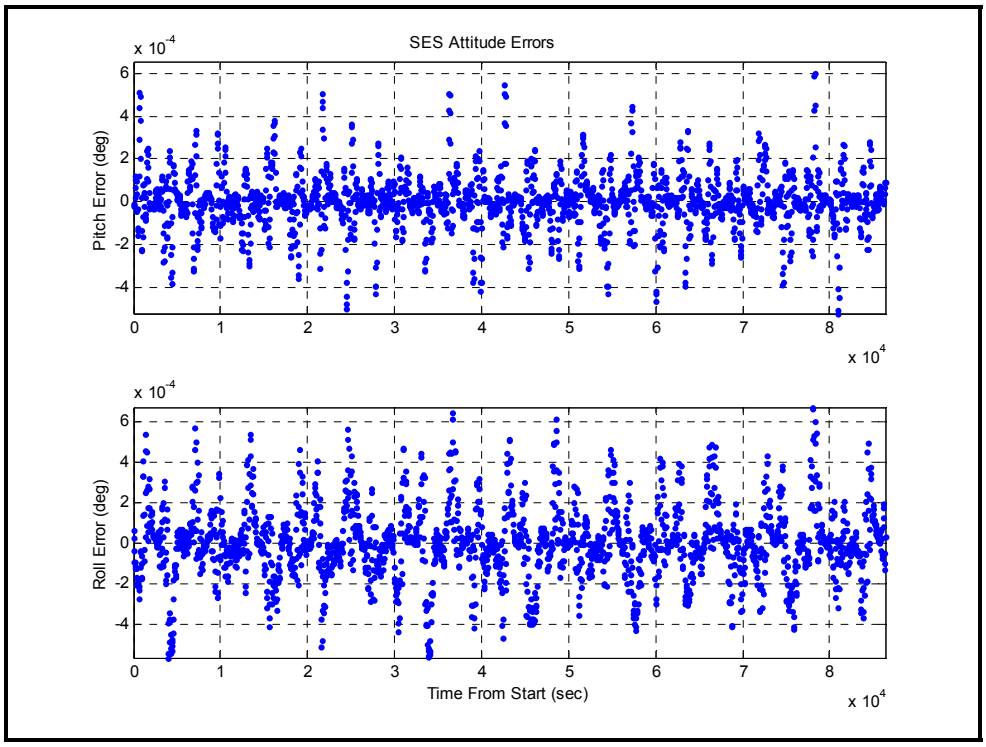

Figure 4. SES Attitude Errors: Case with 4 Clusters, Nominal Yaw, and No Noise

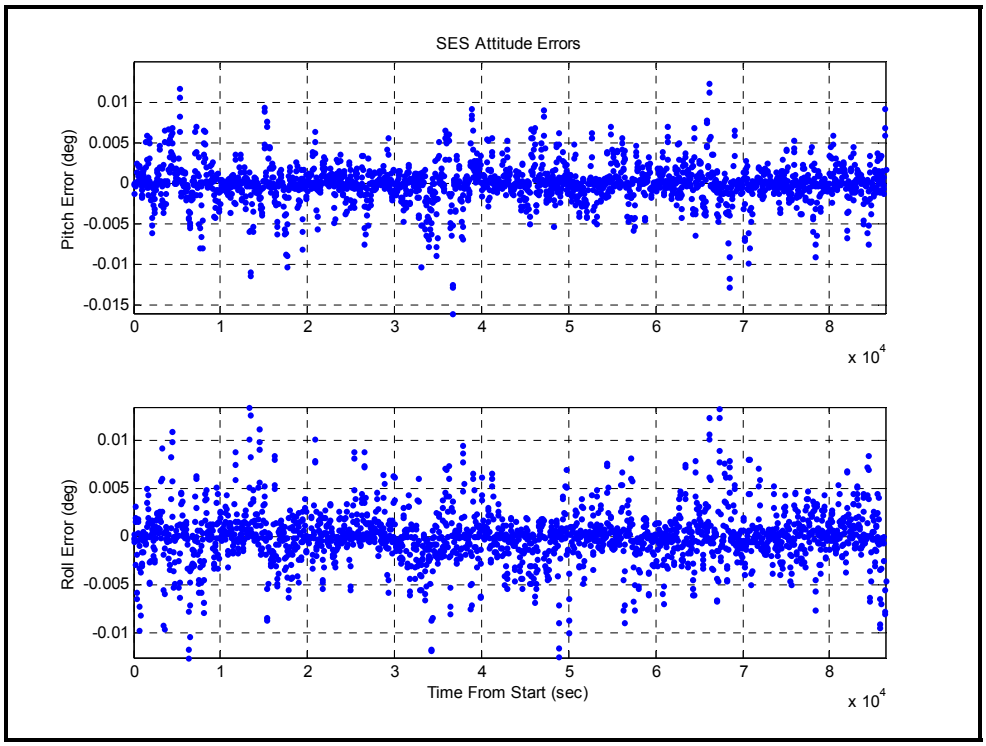

Figure 5. SES Attitude Errors: Case with 4 Clusters, Simulated Unknown Yaw, and No Noise

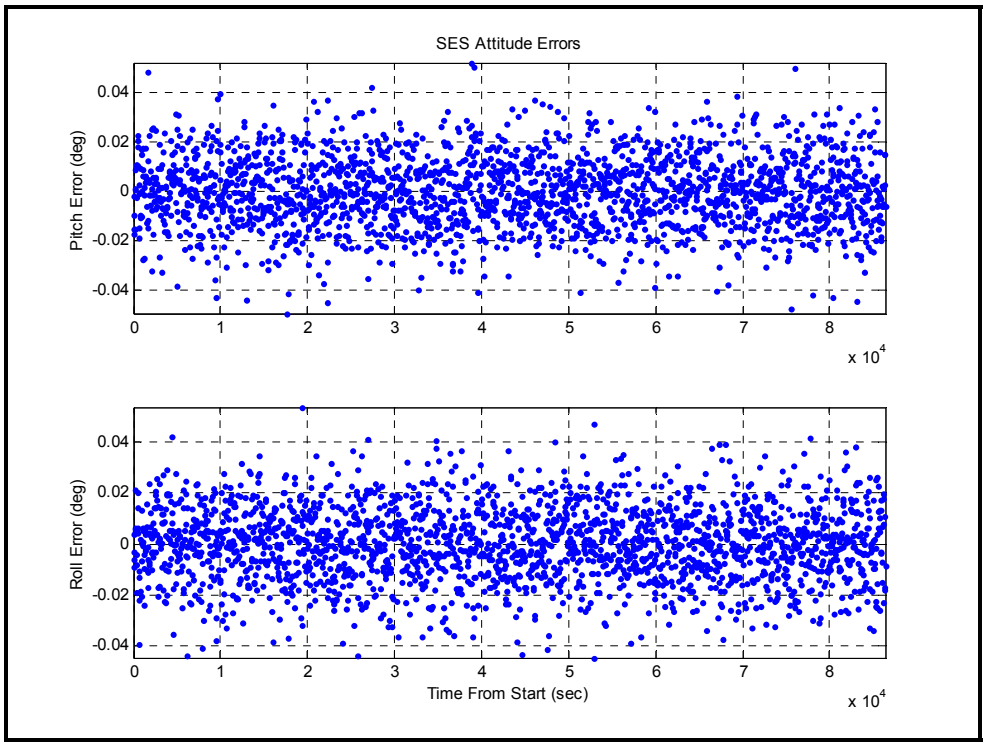

Figure 6. SES Attitude Errors: Case with 4 Clusters, Simulated Unknown Yaw, and 0.02 deg (1σ) Noise

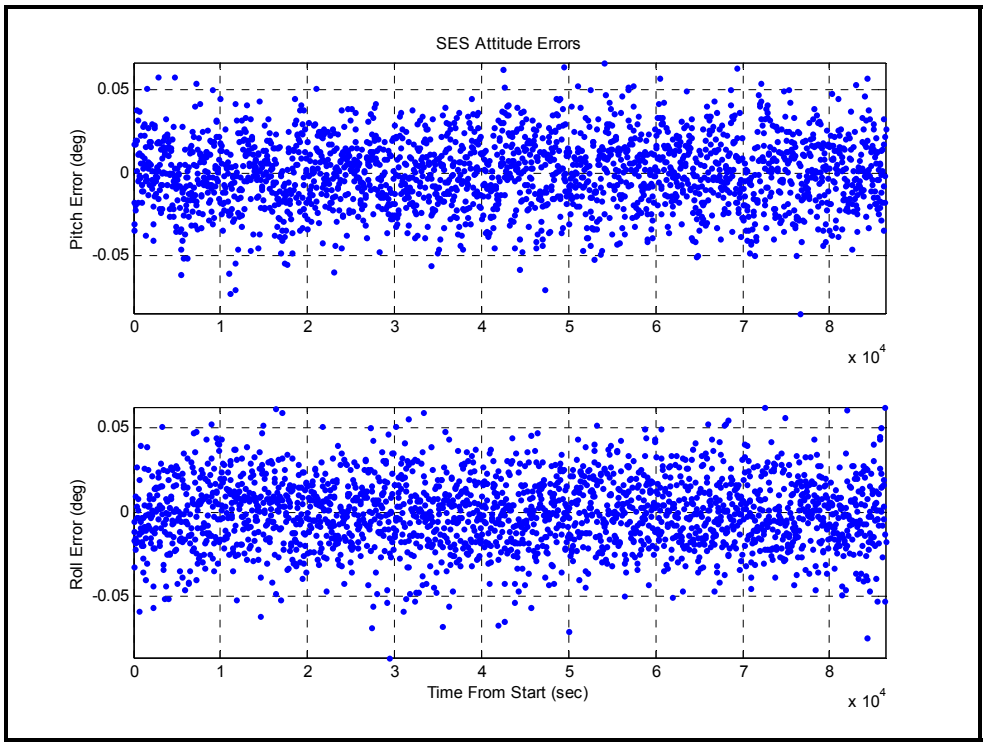

Figure 7 SES Attitude Errors: Case with 2 Clusters, Simulated Unknown Yaw, and 0.02 deg (1σ) Noise

Table 1. Results of SES Attitude Computations

Case	Num. Clusters	Num. Iters.	Noise (deg)	Yaw?	Max |ΔPitch| (deg)	Max |ΔRoll| (deg)	σ |ΔPitch| (deg)	σ |ΔRoll| (deg)	Time (sec)
1	4	1	0.00	0	0.04434	0.02840	0.01698	0.00932	54.3
2	4	2	0.00	0	0.00656	0.00455	0.00253	0.00155	69.7
3	4	3	0.00	0	0.00073	0.00116	0.00031	0.00035	85.4
4	4	4	0.00	0	0.00065	0.00069	0.00013	0.00018	102.8
5	4	5	0.00	0	0.00076	0.00061	0.00016	0.00015	118.9
6	4	6	0.00	0	0.00077	0.00060	0.00017	0.00015	133.3
7	2	1	0.00	0	0.08374	0.00128	0.02241	0.00043	44.7
8	2	2	0.00	0	0.01431	0.00141	0.00490	0.00045	56.2
9	2	3	0.00	0	0.01263	0.00144	0.00598	0.00045	67.9
10	2	4	0.00	0	0.01370	0.00144	0.00630	0.00045	79.7
11	2	5	0.00	0	0.01388	0.00144	0.00635	0.00045	91.9
12	2	6	0.00	0	0.01391	0.00144	0.00636	0.00045	103.2
13	2*	4	0.00	0	0.00160	0.01371	0.00051	0.00627	81.4
14	4	4	0.02	0	0.06311	0.05538	0.01412	0.01423	119.8
15	2	4	0.02	0	0.08439	0.08189	0.02105	0.02000	84.0
16	4	4	0.00	1	0.01603	0.01376	0.00256	0.00286	104.5
17	2	4	0.00	1	0.02329	0.01424	0.00679	0.00291	80.1
18	4	4	0.02	1	0.06178	0.05241	0.01427	0.01451	101.5
19	2	4	0.02	1	0.08740	0.09104	0.02109	0.02012	79.9
20	3	4	0.00	0	0.00094	0.00166	0.00036	0.00043	91.0
21	3	4	0.02	0	0.06456	0.07462	0.01633	0.01629	92.9
22	3	4	0.00	1	0.01427	0.01374	0.00257	0.00292	91.8
23	3	4	0.02	1	0.08599	0.06851	0.01649	0.01668	90.8

* 2 Clusters on the same side of the X-Z plane (for all other cases with 2 clusters, they were on the same side of the Y-Z plane)

Several important results can be seen in Table 1.

1. The algorithm converges after 3 or 4 iterations (In cases 1-6, and 7-12 the errors reach a minimum after 3 or 4 iterations).
2. The inherent 1-σ accuracy of the method is better than 0.0002 deg for four clusters (case 4), about 0.0004 deg for three clusters (case 20), and about 0.006 deg for 2 clusters (case 9).
3. The geometry of the clusters greatly affects the accuracy—for the geometries used in the simulation, and using 2 clusters, calculated values of rotations about an axis between the clusters were an order of magnitude more accurate than those about an axis perpendicular to the cluster bisector (cases 10 and 13).
4. If the (unobservable) yaw is not known from other sensors and is not small (<< 1 deg) the accuracy decreases to about 0.003 deg for the four (case 16) and three cluster (case 22) cases, and to as much as 0.007 deg for the 2 cluster case (case 17).

5. Addition of noise (0.02 deg 1σ) produces errors equal to the noise for the two cluster case (case 15 and 19), and approximately equal to the noise divided by the square root of 2 for the four cluster case (case 14 and 18). For the three cluster case introduction of noise caused errors only slightly greater than those for the four cluster case (compare cases 21 and 23 with cases 14 and 18).
6. The noise is the major overall error source (compare cases 14, 16 and 18 for four clusters, cases 15, 17, and 19 for two clusters, and cases 21, 22, and 23 for 3 clusters).
7. The current implementation of the algorithm can process about 200 observations per second on a personal computer operating at 833 MHz. The most time consuming portions of the code are retrieving the ephemeris and solving for the attitude with the QUEST algorithm.

Even with no applied noise and perfect knowledge of yaw, the computed pitch and roll values contain small, but noticeable errors. The following discussion shows why the approximation that the roll and pitch measurements are independent yield small, but finite, errors. For example, if a cluster is in the X-Z plane, its penetration angle is assumed to be independent of rotations about the X-axis and proportional to rotations about the Y-axis. The error in this approximation is illustrated in Figure 8.

Figure 8 shows the Earth occultation of the central eye in an SES cluster in the body X-Z plane such that $\hat{Y}_C \equiv \hat{X}$. This cluster is sensitive to rotations about the Y-axis and should be insensitive to rotations about the X-axis. Two cases are shown: in the FOV on the left, the X-axis rotation (Φ) is zero, while on the right it is significant. The point A is on the X-axis while B and C are on the Earth limb, at the center of the FOV, for the two cases. Note that all of the angles have been exaggerated to illustrate the effect. Measured penetration angles are proportional to the total occulted area (shaded in the figure). In this algorithm, modeled penetration angles are the angles from the reference point (on the base of the triangular eye—see Fig 2) to the intersection of the Earth limb with the normal to the base of the FOV (points C and B for the two cases).

When Φ is zero, rotations about Y move the FOV so that the Earth penetrates it to a degree proportional to the rotation angle. For Φ not equal to zero, two effects occur: 1) the position of the Earth limb intersection changes (points B and C) so that for the same Y-rotation a different penetration angle is observed; 2) the shape (and area) of the Earth occultation area changes.

For near nominal attitudes, the angle from the body X-axis to Nadir (not shown) is nearly 90 deg. The angle (ϕ) from nadir to the Earth limb at B is nearly independent of Φ so the angle (λ) from the X-axis to B is given by:

$$\sin\lambda = \frac{\cos\phi}{\cos\Phi} \tag{11}$$

If the X-axis is 90 deg from nadir, a rotation about it of 1.5 deg (e.g., Φ = 1.5 deg) results in a change of λ, and therefore the penetration angle, of about 0.01 deg.

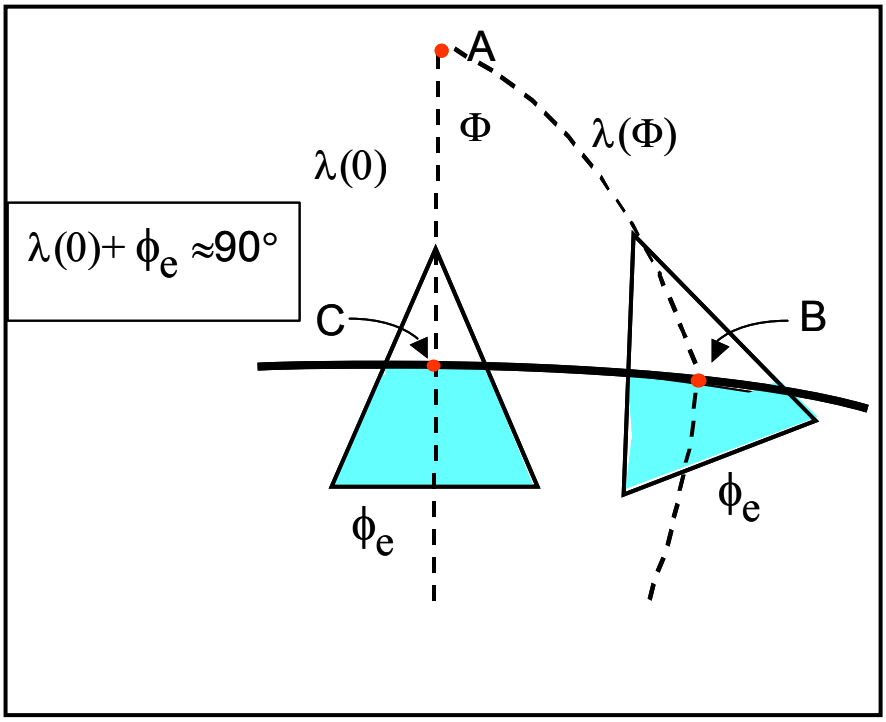

Figure 8. Effect of Rotation on Penetration Angle

The second effect is illustrated in Figure 9. This figure illustrates a trapezoidal portion of an FOV with internal angle α. The Earth limb (approximated as straight dashed lines) is drawn for a nominal case (line BE) and a case with a rotation of Φ (line AD). The detected penetration angle is proportional to the area under BE in the one case and under AD in the other. Using plane geometry and the tangent to the Earth limb, instead of the limb itself, as close approximations, the area of triangle ABC is:

$$AREA(ABC) = \frac{r^2 \sin(\Phi)\sin(\alpha)}{2\sin(\alpha + \Phi)} \tag{12}$$

where r is the length of CB (= length of CE). The area of triangle CDE is:

$$AREA(CDE) = \frac{r^2 \sin(\Phi)\sin(\alpha)}{2\sin(\alpha - \Phi)} \tag{13}$$

The occulted area is:

$$AREA(occulted) = \left(\frac{b^2}{4} - r^2\right)\tan(\alpha) \tag{14}$$

where b is the length of the base of the eye.

For typical geometry parameters (α = 60 deg, r = 2 deg, b = 5 deg), and Φ ≈ 2 deg, the difference of the triangles' areas is on the order of 0.01 percent of the occulted area. This would produce an error of the same size in the measured penetration angle.

Reference 3 contains a more complete description of these approximations.

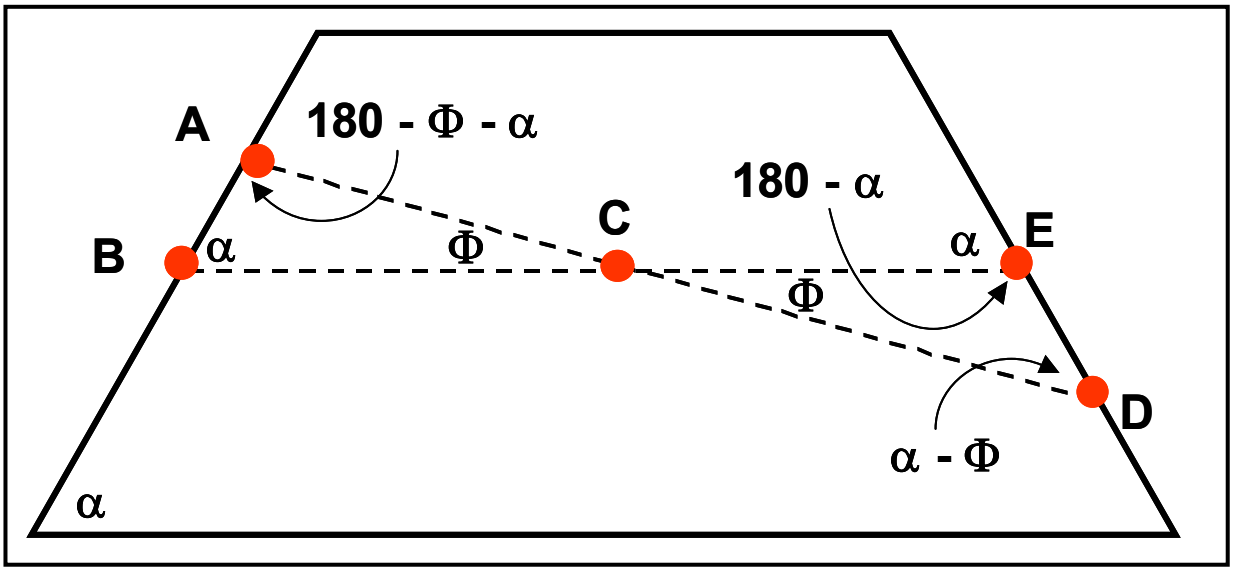

Figure 9. Illustration of Change in Detected Earth Area With Rotation About Non-sensitive Axis

CONCLUSIONS

Although the algorithm presented here does not provide exact results, the error inherent in the algorithm is smaller than SES measurement errors. The largest component of SES error comes from the variation of the Earth limb height.[8] Although part of this variation is systematic, varying with latitude and season, the stochastic, correlated portion can change the Earth limb height by ±5 km or more.[9,10] At an altitude of 700 km, this results in an unpredictable variation in penetration angles of about ±0.1 deg. If such errors were distributed uniformly, their standard deviation would be about 0.06 deg.

In this study the simulated noise led to penetration angle errors of 0.02 deg, about 1/3 of the typical values at this altitude. Even at this low level, these variations were the principal source of error. In addition, for a well controlled spacecraft, the pitch and roll would be significantly closer to nominal, and the yaw known more accurately, than was modeled in this study. These factors would further reduce the errors due to the algorithm, as compared to those due to unpredictable variations.

The major advantage of the new algorithm is its generality.

The same algorithm can be used for Static Earth Sensors, regardless of the number or placement of the clusters. No special modification of the algorithm is needed if clusters fail or during periods of Sun or Moon interference.

Several refinements and related applications could be developed.

Allowing variable cluster weights might improve the method's accuracy. The weights could be chosen based on predicted horizon height uncertainties at the time and location of each Earth horizon measurement.

A variation on this algorithm could be developed for scanning Earth sensors. Scanning Earth sensors view the Earth limb by rotating an infrared sensitive detector around an axis so that its FOV intersects the Earth at two points. The position of these two points in the body frame can

be computed from raw sensor data and treated in the same way that the observations from the SES clusters are in the method described here.

It would also be possible to use horizon crossing vectors directly in an extended Kalman filter. This would eliminate the conventional intermediate step of first computing observed nadir vectors. In order to use horizon crossing vectors directly, it would be necessary for the filter to take account of the different uncertainties in the vector components.

REFERENCES

1. "TRMM Earth Sensor Assembly Technical User's Manual, Model 13-401, CDRL 7B, SOW 4.1," prepared by EDO Corporation Barnes Engineering Division, NASA Contract No. NAS5-32463, June 1995

2. B. Robertson, S. Placanica, W. Morgenstern, J. Hashmall, J. Glickman, and G. Natanson, "On-Orbit Performance of the TRMM Mission Mode," J*ournal of the Brazilian Society of Mechanical Sciences, Vol. 21 (Special Issue: Proceedings of the 14th International Symposium on Space Flight Dynamics),* Feb. 1999, pp. 238-249

3. G. Natanson, "Ground-Support Algorithms for Simulation, Processing, and Calibration of Barnes Static Earth Sensor Measurements: Application to the Tropical Rainfall Measuring Mission Laboratory," *Proceedings of the Flight Mechanics Symposium*, NASA Conference Publication No. 3345, Goddard Space Flight Center, Greenbelt, MD, May 1997

4. M. Challa and G. Natanson, "Recent Developments in Earth Oblateness Modeling for Attitude Determination," *Journal of the Brazilian Society of Mechanical Sciences, Vol. 21 (Special Issue: Proceedings of the 14th International Symposium on Space Flight Dynamics)*, Feb. 1999, pp. 134-144

5. G. Natanson, "Accuracy of Earth Pointing Using Adjacent Quadrants of the Barnes Static Earth Sensor: Analysis of Flight Data From the Tropical Rainfall Measuring Mission (TRMM)," Technical Memorandum, CSC-96-968-03, Computer Sciences Corporation, January 2000

6. J. Glickman, "Earth Observing System-PM1 (EOS-PM1) / Aqua, Postlaunch Report," Prepared by Computer Sciences Corporation for NASA/GSFC, February 2003

7. M. D. Shuster and S. D. Oh, "Three-Axis Attitude Determination from Vector Observations," *Journal of Guidance and Control*, Vol. 4, 1981, pp.70-77

8. E. Harvie, O. Filla, and D. Baker, "In-Flight Measurement of the National Oceanic and Atmospheric Administration (NOAA)-10 Static Earth Sensor Error," *AAS/AIAA Spaceflight Mechanics Meeting*, Pasadena, California, February 22–24, 1993

9. J. Hashmall, J. Sedlak, D. Andrews, and R. Luquette, "Empirical Correction for Earth Sensor Horizon Radiance Variation," *Spaceflight Dynamics 1998-Advances in the Astronautical Sciences*, Vol. 100, May 1998, pp 453-468

10. S. Sallard, G. Samson, J. Krebs, P. Faucher-Lagracie, P. Prieur, and M. Burello, "New Accurate Infrared Earth Radiance Model for Pointing Accuracy Improvement of LEO Platforms," *Spaceflight Dynamics 1998-Advances in the Astronautical Sciences*, Vol. 100, May 1998, pp. 469-484